

UC Davis

UC Davis Previously Published Works

Title

Identification of Resistance Pathways Specific to Malignancy Using Organoid Models of Pancreatic Cancer

Permalink

<https://escholarship.org/uc/item/6k28v7vh>

Journal

Clinical Cancer Research, 25(22)

ISSN

1078-0432

Authors

Ponz-Sarvise, Mariano
Corbo, Vincenzo
Tiriac, Hervé
[et al.](#)

Publication Date

2019-11-15

DOI

10.1158/1078-0432.ccr-19-1398

Peer reviewed



Published in final edited form as:

Clin Cancer Res. 2019 November 15; 25(22): 6742–6755. doi:10.1158/1078-0432.CCR-19-1398.

Identification of Resistance Pathways Specific to Malignancy Using Organoid Models of Pancreatic Cancer

Mariano Ponz-Sarvise^{1,2,*†}, Vincenzo Corbo^{1,2,*^}, Hervé Tiriach^{1,2,*}, Dannielle D. Engle^{1,2,*@}, Kristopher K. Frese^{3,*}, Tobiloba E. Oni^{1,2,4}, Chang-II Hwang^{1,2,^^}, Daniel Öhlund^{1,2,+}, Iok In Christine Chio^{1,2,++}, Lindsey A. Baker^{1,2}, Dea Filippini^{1,2,^}, Kevin Wright^{1,2}, Tashinga E. Bapiro^{8,\$}, Pearl Huang⁹, Paul Smith^{\$}, Kenneth H. Yu^{1,2,5,6}, Duncan I Jodrell^{7,8}, Youngkyu Park^{1,2,10}, David A. Tuveson^{1,2,10}

¹Cold Spring Harbor Laboratory, Cold Spring Harbor, NY, USA

²Lustgarten Pancreatic Cancer Research Laboratory, Cold Spring Harbor, NY, USA

³Cancer Research UK Manchester Institute, Manchester, UK

⁴Graduate Program in Molecular and Cellular Biology, Stony Brook University, Stony Brook, NY, USA

⁵Rubenstein Center for Pancreatic Cancer Research, Memorial Sloan Kettering Cancer Center, New York, NY 10065, USA

⁶Weill Medical College at Cornell University, New York, NY, USA

⁷Cancer Research UK Cambridge Institute, The University of Cambridge, Li Ka Shing Centre, Cambridge, UK

Corresponding Authors: Youngkyu Park, Cold Spring Harbor Laboratory, One Bungtown Road, Cold Spring Harbor, NY 11724, (516) 367-6856, ypark@cshl.edu; David A. Tuveson, Cold Spring Harbor Laboratory, One Bungtown Road, Cold Spring Harbor, NY 11724, (516) 367-5246, dtuveson@cshl.edu. ¹⁰Co-corresponding authors.

^{*}Co-first authors

[†]Current address: Department of Oncology, Clinica Universidad de Navarra, CIMA, IDISNA, Pamplona, Spain

[^]Current address: Department of Diagnostics and Public Health, University of Verona, Verona, Italy

^{^^}Current address: Department of Microbiology and Molecular Genetics, University of California, Davis, CA, USA

⁺Current address: Department of Radiation Sciences and Wallenberg Centre for Molecular Medicine, Umeå University, Umeå, Sweden

⁺⁺Current address: Institute for Cancer Genetics, Columbia University Medical Center, New York, NY, 10032 USA

^{\$}Current address: IMED Biotech Unit, AstraZeneca, Cambridge, United Kingdom

[@]Current address: The Salk Institute for Biological Studies, La Jolla, CA, USA

Author contributions:

- Conception and design: MPS, VC, HT, DDE, KKF, PH, PS, YP and DAT
- Development of methodology: MPS, VC, HT, DDE
- Acquisition of data: MPS performed *in vitro* cytotoxicity assays with organoids; KKF, MPS, DF, KW, BD, YP performed *in vivo* experiments using KPC mice; CH, IICC, DO, DDE, HT, KY, and YP generated mouse and human organoids; DDE, HT, KW, BD, YP performed human organoid *in vivo* transplantation experiments; HT, DDE performed IHC and quantification analyses. MPS, VC, HT, KKF, TO performed western blot, phospho-RTK array, and qRT-PCR analyses; TB and DIJ performed the pharmacokinetic experiments with KKF.
- Analysis and interpretation of data (e.g., statistical analysis, biostatistics): MPS, VC, HT, DDE, KKF, TB, DIJ and DAT
- Writing, review, and/or revision of the manuscript: DDE, MPS, VC, HT, LAB, YP and DAT co-wrote the manuscript. All authors commented on the manuscript and approved final version.
- Study supervision: MPS, VC, HT, DDE, KKF, YP and DAT

Conflict of Interest Statement: The authors declare no potential conflicts of interest.

⁸Department of Oncology, University of Cambridge, Cambridge, UK

⁹Cygnal Therapeutics, Boston, MA

Abstract

Purpose: *KRAS* is mutated in the majority of pancreatic ductal adenocarcinoma. MAPK and PI3K-AKT are primary *KRAS* effector pathways, but combined MAPK and PI3K inhibition has not been demonstrated to be clinically effective to date. We explore the resistance mechanisms uniquely employed by malignant cells.

Experimental Design: We evaluated the expression and activation of receptor tyrosine kinases in response to combined MEK and AKT inhibition in KPC mice and pancreatic ductal organoids. Additionally, we sought to determine the therapeutic efficacy of targeting resistance pathways induced by MEK and AKT inhibition in order to identify malignant-specific vulnerabilities.

Results: Combined MEK and AKT inhibition modestly extended the survival of KPC mice and increased Egfr and ErbB2 phosphorylation levels. Tumor organoids, but not their normal counterparts, exhibited elevated phosphorylation of ERBB2 and ERBB3 after MEK and AKT blockade. A pan-ERBB inhibitor synergized with MEK and AKT blockade in human PDA organoids, whereas this was not observed for the EGFR inhibitor Erlotinib. Combined MEK and ERBB inhibitor treatment of human organoid orthotopic xenografts was sufficient to cause tumor regression in short-term intervention studies.

Conclusions: Analyses of normal and tumor pancreatic organoids revealed the importance of ERBB activation during MEK and AKT blockade primarily in the malignant cultures. The lack of ERBB hyperactivation in normal organoids suggests a larger therapeutic index. In our models pan-ERBB inhibition was synergistic with dual inhibition of MEK and AKT and the combination of a pan-ERBB inhibitor with MEK antagonists showed the highest activity both *in vitro* and *in vivo*.

STATEMENT OF TRANSLATIONAL RELEVANCE

Therapeutic strategies for pancreatic ductal adenocarcinoma (PDA) are largely ineffective. *Kras* signaling is aberrantly activated but has proven a difficult clinical target. Dual inhibition of the two *KRAS* effectors, AKT and MAPK, failed in clinical trials due in part to the rapid development of resistance. The KPC mouse model of PDA is resistant to dual MEK and AKT inhibition and activates Egfr and ErbB2 *in vivo*. Using organoids, we explore the differential response of non-neoplastic and PDA cells to MEK and AKT inhibition. Hyper-activation of the ErbB pathway was observed in the neoplastic, but not normal organoids in response to dual MEK and AKT blockade. Inhibition of MEK and ERBB was synergistic and resulted in tumor regressions in an orthotopic xenograft model. These data suggest that combined inhibition of MEK and ERBB may be able to achieve therapeutic index. Together, these data demonstrate that the three-dimensional organoid culture system is a platform to interrogate the effects of targeted therapies in both neoplastic and non-transformed cells and can complement standard genetically engineered mouse and transplantation models.

INTRODUCTION

Pancreatic ductal adenocarcinoma (PDA) is a deadly disease with a 5-year survival rate of less than 8% [1]. This dismal prognosis results from late diagnoses and limited efficacy of systemic treatments [2]. *KRAS* mutation is detected in more than 90% of PDA [3]. The majority of mutations are substitutions in codons 12-13 that cause persistent *KRAS* activation [4]. Activated *KRAS* engages a multitude of pathways that regulate cellular processes such as proliferation and cell survival [4]. The importance of *KRAS* mutations in PDA tumorigenesis and maintenance has been extensively demonstrated in genetically engineered mouse models (GEMMs) [5–7].

While recent attempts to pharmacologically target *KRAS* have yielded modest success in the setting of G12C mutation [8], this mutation is uncommon in pancreatic cancer [9] and *KRAS* has otherwise proven difficult to target [10]. Therefore, alternative approaches have often focused on developing agents that target two downstream effector pathways, the MAPK and the PI3K signaling cascades [10].

However, marginal or no activity has been observed following the combined inhibition of MAPK/ERK and PI3K/AKT pathways in GEMMs [11, 12], xenografts [13, 14], and a phase II clinical trial [13, 15]. Targeting of MEK and AKT signaling with selumetinib (AZD6244) and MK2206 was tested in *KRAS*-driven human malignancies in phase I clinical trial (). Among 29 enrolled patients, there was one PDA patient who achieved a marginal response, albeit the patient's *KRAS* status was unknown [13]. Additionally, dual inhibition of MEK and AKT did not improve overall survival in PDA patients for whom gemcitabine-based chemotherapy had failed in randomized phase II clinical trial () [15]. The existence of complex feedback mechanisms when individually inhibiting MEK or AKT has been reported [16–21] and include the activation of a number of Receptor Tyrosine Kinases (RTKs) (including ERBB receptors), explaining the low efficacy of agents targeting these individual pathways in PDA and other malignancies [16–21]. Therefore, we sought to better understand the alterations in cellular signaling that occur upon dual MEK and AKT blockade in PDA and to determine whether these responses are found in both normal and malignant ductal cells.

The evaluation of therapeutic efficacy in PDA has often relied on monolayer cultures, which does not support the proliferation of non-transformed, normal pancreatic ductal cells. We sought to determine whether resistance to targeted therapy was a unique property of cancer cells or if this property was a common response to targeting these pathways in ductal cells. To directly compare normal and neoplastic responses to targeted therapy, we developed a three-dimensional organoid model system to propagate pancreatic cells from either neoplastic or non-neoplastic tissues [22, 23]. Using the organoid model system, we compared the response of normal and malignant cells to combined MEK and AKT inhibition. Within the same media conditions for both cell types, we identified feedback mechanisms specific to neoplastic cells. A better understanding of how non-transformed cells respond to these targeted agents may help to identify therapeutic combinations that are less toxic when administered to patients.

In this study, we investigated the efficacy of the dual inhibition of MEK (selumetinib) and AKT (MK2206) in PDA using *Kras^{+/LSL-G12D}; Trp53^{+/LSL-R172H}; Pdx1-Cre* (KPC) mice [24] as well as in mouse and human pancreatic organoid and monolayer cultures [22]. Herein, we show that both mouse and human PDA-derived organoids recapitulate the modest efficacy of the combined MEK and AKT inhibitor treatment *in vivo*. Increased IGF-1R and INS-R phosphorylation was observed after dual MEK and AKT inhibition in both untransformed and malignant cells, indicating that activation of these receptor tyrosine kinases (RTKs). In contrast, hyper-activation of the ERBB pathway was unique to malignant organoids and was not observed in their normal counterparts. Our study suggests that targeting the ERBB pathway may have fewer side effects than targeting the IGF-1R or INS-R pathways and be able to achieve a higher therapeutic index. Interruption of this feedback loop using a pan-ERBB kinase inhibitor resulted in synergistic suppression of cell viability *in vitro* and tumor regressions *in vivo* when combined with MEK inhibition.

MATERIALS AND METHODS

Cell culture

Cell lines were derived from our murine KPC tumors and maintained in DMEM (41966029, Invitrogen) with 10% FBS (SH30070.03, HyClone). Protein lysates were obtained using RIPA buffer with protease and phosphatase inhibitors. AZD6244 (ARRY-142886, Selumetinib, AstraZeneca) and MK2206 (Merck) were dissolved in DMSO. Gemcitabine (Addenbrookes, Memorial Sloan Kettering Cancer Center) was dissolved in saline, and used as indicated. Cell viability experiments were performed via Cell Titer-Glo (G7570, Promega) according to manufacturers recommended protocols.

Organoid isolation and culture

Detailed procedures to isolate and propagate mouse and human, normal and neoplastic pancreatic organoids have been described previously [22, 25]. In brief, normal pancreatic mouse ducts were manually picked after enzymatic digestion of pancreas with 0.012% (w/v) collagenase XI (Sigma) and 0.012% (w/v) dispase (GIBCO) in DMEM media containing 1% FBS (GIBCO) and were seeded in growth factor-reduced (GFR) Matrigel (BD). For tumors (mT), bulk tissues were minced and digested overnight with collagenase XI and dispase and embedded in GFR Matrigel. In the case of human primary and metastatic pancreatic tumor organoid cultures (hT), tumor tissue was minced and digested with collagenase II (5 mg/ml, GIBCO) in human complete medium at 37°C for a maximum of 16 hours. The material was further digested with TrypLE (GIBCO) for 15 minutes at 37°C, and embedded in GFR Matrigel. Normal samples were processed as above, except that the collagenase digestion was done for a maximum of 2 hours in the presence of soybean trypsin inhibitor (1 mg/ml, Sigma).

Animals

Trp53^{+/LSL-R172H}, Kras^{+/LSL-G12D} and Pdx1-Cre strains on a C57Bl/6 background were interbred to obtain *Pdx1-Cre; Kras^{+/LSL-G12D}; Trp53^{+/LSL-R172H}* (KPC) mice [24]. C57Bl/6 mice were purchased from the Jackson Laboratory. For human tumor organoid xenograft experiments, immunocompromized (NOD *scid* gamma (NSG), Jax stock number 005557)

were used. All animal experiments were conducted in accordance with procedures approved by the Institutional Animal Care and Use Committee (IACUC) at Cold Spring Harbor Laboratory and the Home Office license and the Cambridge Research Institute Ethics committee in Cambridge, UK.

Therapeutic experiments with organoids

Neratinib, MK2206 and selumetinib (Selleck) were dissolved in DMSO. The final concentration of DMSO was no higher than 0.2%. The following doses were used for the cytotoxicity assay: neratinib and MK2206: 1 nM, 5 nM, 10 nM, 50 nM, 100 nM, 500 nM, 1 μ M, 5 μ M, 10 μ M, 100 μ M; selumetinib: 10 nM, 20 nM, 100 nM, 200 nM, 1 μ M, 2 μ M, 10 μ M, 20 μ M, 100 μ M, 200 μ M. When combinations of drugs were used, the EC50 of each drug alone was determined in the organoid lines, and the ratio of the two EC50s was calculated. Dose ranges of each drug were then calculated, keeping this EC50 ratio constant [26].

For EC50 analysis, organoids were dissociated to single cells by triturating organoids in media through a fire-polished glass pipette, and then by enzymatic dissociation with 2 mg/mL dispase dissolved in TrypLE (Life Technologies) at 37 C, until the organoids appeared as single cells under the microscope (15-45 minutes). Cells were counted, and diluted to 10-30 cells/ μ L in a mixture of complete media, Rho Kinase inhibitor Y-27632 (10.5 μ M final concentration, Sigma), and GFR Matrigel (10% final concentration). 100 μ L of this mixture (1000-3000 cells per well) was plated in a 96-well plate (Nunc) previously coated with a bed of GFR Matrigel. Once organoids reformed (between 36-48 hours post-plating, confirmed by microscopy), drugs were added in 100 μ L of media. Ten different doses plus a vehicle control were used for each drug, and five replicate wells were treated with each dose. 72 hours after the addition of the drug, cell viability was measured using a luminescence ATP-based assay (CellTiter-Glo, Promega) and a plate reader (I3, Molecular Devices). The curves shown in the figures and the calculated IC50 values for both human and mouse were the result of three biological replicates for each type of organoid.

For signaling pathway analysis, including western blots, RTK arrays and qRT-PCR, organoids were seeded as fragments in complete media. After 24 hours, media was changed with media containing 1 μ M of the indicated drug or drugs. DMSO was used as vehicle control. Where indicated, organoids were evaluated after 60 hours instead of 72 hours to recover sufficient material for protein analyses.

Therapeutic intervention studies in mice.

Detailed information about the study design and tumor monitoring were described previously [27]. Briefly, upon detection of a mass during weekly manual palpation, KPC mice were subjected to high-contrast ultrasound imaging using the Vevo 2100 System with a MS250, 13–24 MHz scanhead (Visual Sonics, Inc, Amsterdam, NL). KPC mice with tumor diameters of 5–9 mm were randomized and enrolled into the therapeutic intervention studies according to the outlined treatment schedules. NSG mice were surgically implanted with human tumor organoids between 8 – 12 weeks of age. In short, organoids were dissociated into single cells and transplanted into the pancreas in 50 μ L of 50% GFR Matrigel. Upon

reaching clinical endpoint, the engrafted tumors were passaged into new NSG host pancreata as 2mm³ fragments using tissue glue (Vetclose, Henry Schein). Human tumor organoid xenografts, passage 1, were enrolled in therapeutic intervention studies upon reaching greater than 350mm³ in size. Selumetinib (AZD6244, ARRY-142886, AstraZeneca) and MK2206 (Merck) were formulated in 0.5% methylcellulose. Mice were administered methylcellulose vehicle, 25 mg/kg selumetinib bidaily, and/or 100 mg/kg MK2206 every other day or 50 mg/kg neratinib daily via oral gavage [13, 28, 29]. Gemcitabine was administered intraperitoneally at a dose of 100mg/kg [30].

Pharmacokinetic analyses

Fresh frozen tumor samples and cell pellets were processed and analyzed as previously described[31]. Briefly, gemcitabine LC-MS/MS was performed on a TSQ Vantage triple stage quadrupole mass spectrometer (Thermo Scientific, USA) fitted with a heated electrospray ionization (HESI-II) probe operated in positive and negative mode at a spray voltage of 2.5 KV, capillary temperature of 150°C. Quantitative data acquisition was done using LC Quan2.5.6 (Thermo Fisher Scientific, USA). MK2206 HPLC-MS/MS was performed at Merck Research Labs, Tsukuba, Ibaraki, Japan.

Histology

Tissues were fixed in 10% neutral buffered formalin and embedded in paraffin. Sections were subjected to immunohistochemical staining using the following primary antibodies: Cleaved Caspase-3 (9661, Cell Signaling), phospho-histone H3 (3377, Cell Signaling) and Ki67 (D2H10, Cell Signaling).

Western blot analysis

Organoids were harvested using Cell Recovery Solution (Corning) on ice. Organoids were lysed using boiling SDS-lysis buffer (50mM Tris-HCL [pH 7.4], 2% SDS). Protein lysates were separated using 4-12% Bis-Tris NuPage gels (Life Technologies). Isolation of protein from hN organoids following treatment with MEK and AKT antagonists required time points of 48 hours or less in order to obtain sufficient protein quantities. Western blots were probed with the following antibodies: phospho-ERK1/2 (4370, Cell Signaling), pan-ERK1/2 (4695, Cell Signaling), phospho-Akt (4060, Cell Signaling), pan-Akt (4685, Cell Signaling), phospho-ribosomal S6 (4858, Cell Signaling), S6 Ribosomal Protein (2317, Cell Signaling), pan-EGFR (Abcam, ab2430), phospho-EGFR (3777, Cell Signaling) ERBB2 (4290, Cell Signaling), phospho-ERBB2 (2247, Cell Signaling), ERBB3 (12708, Cell Signaling), phospho-ERBB3 (4791, Cell Signaling) Heat Shock Protein 90 (07-2174, Millipore or 4874, Cell Signaling), actin (sc-1616, Santa Cruz Biotechnologies) and Kras (sc-30, Santa Cruz Biotechnologies). Loading control for western blot is Hsp90 unless otherwise indicated.

Receptor tyrosine kinase antibody arrays

Mouse Phospho-Receptor Tyrosine Kinase (RTK) Arrays (ARY014, R&D Systems) and Human Phospho-Receptor Tyrosine Kinase (RTK) Arrays (ARY001B, R&D Systems) were used. Tumors or organoids were processed according to manufacturer's recommendations and 200 µg of lysates from tumors treated for 7 days with Gemcitabine or with MEKi +

AKTi + Gemcitabine (n = 3 mice per group) were incubated with arrays overnight at 4°C. Multiple exposures were used to determine optimal sensitivity and films were scanned using trans-illumination. Data was quantified using ImageJ. For each, phospho-protein fold induction relative to experimental controls was determined.

Quantitative reverse transcription polymerase chain reaction (qRT-PCR)

RNA was extracted from cell cultures or freshly isolated tissues using TRIzol (Invitrogen), followed by column-based purification with the PureLink RNA Mini Kit (Ambion). cDNA was synthesized using 1 µg of total RNA and TaqMan Reverse Transcription Reagents (Applied Biosystem). All targets were amplified (40 cycles) using gene-specific Taqman primers and probe sets (Applied Biosystems) on a 7900HT Real time-PCR (Applied Biosystem). Relative gene expression quantification was performed using the Ct method with the Sequence Detection Systems Software, Version 1.9.1 (Applied Biosystems). Levels of each gene were normalized to *HPRT*, and then levels of genes following treatment were normalized to those of the vehicle control.

Dual-drug combination assay

Organoids were plated in 96-well plates and treated with various concentrations of kinase inhibitors, either alone or in combination for 72 hours. Cell viability was determined as described above. Synergistic effects were determined by using the Chou–Talay method to calculate the combination index (CI) [26]. CIs of <1, 1, and >1 indicate synergism, additive effect, and antagonism, respectively. At least two independent experiments with five replicates were performed.

Statistical analysis

Statistical analysis was performed using GraphPad Prism version 6 (GraphPad, La Jolla, CA, USA). All results are expressed as mean ± SEM unless otherwise indicated. Comparisons between groups were performed with the Student t-test or with the Mann-Whitney non-parametric t-test as required. Kaplan–Meier curves and the log-rank test were used to analyze differences in survival time. For the dose-response curves, the luminescence data was first normalized to the vehicle control and then analyzed using nonlinear regression. For the qRT-PCR experiments, the Holm-Sidak method was used to perform multiple t tests at once. Error bars indicate standard deviation of the means. * p<0.05, ** p<0.01, and ***p<0.001 relative to vehicle control by multiple t test with correction for multiple comparisons. For the Western Differences were considered significant at a p value <0.05 and the values presented in the figures are p<0.05, ** p<0.01, and ***p<0.001.

RESULTS

The combined inhibition of MEK and AKT shows modest efficacy in a mouse model of PDA

To determine if the KPC mouse model accurately recapitulated the MEK and AKT inhibitor (MEKi and AKTi, respectively) responses observed in patients and by other investigators, we performed a short-term intervention study (7 days, supplementary figure 1A) of MEKi, AKTi, or both, in the presence or absence of gemcitabine (Gem). Treatment of tumor-bearing KPC mice with MEKi and AKTi effectively attenuated the targeted pathways (figure

1A). Compensatory hyper-phosphorylation of ERK or AKT was observed upon single agent treatment with AKTi or MEKi, respectively, but treatment with both inhibitors results in attenuation of both signaling pathways (figure 1A). Addition of Gem to these short-term treatment regimens reduced the proliferation status of the tumors while the triple combination of MEKi, AKTi, and Gem significantly induced apoptosis (figures 1B, 1C). These data show that the combination of MEKi and AKTi leads to transient responses.

In a survival study setting, Gem or MEKi monotherapy did not significantly impact tumor growth or survival, whereas AKTi single agent administration reduced tumor growth but without extension in survival (figures 1E and supplementary figures 1B – E). However, when Gem was administered in combination with either AKTi or MEKi, there was a substantial decrease in tumor growth compared to vehicle control or Gem monotherapy (figure 1D). This reduction in tumor growth translated to a significant albeit modest increase in survival in the AKTi + Gem cohort (supplementary figures 1D, 1E). The reduction in tumor growth upon combination therapy of MEKi and AKTi translated into a modest prolongation of the survival when compared to the vehicle control or Gem monotherapy (median survival = 21 versus 11 days, MEKi + AKTi and Gem, respectively; $p = 0.037$) (figures 1E and supplementary figures 1D, 1E). Tumor regressions were elicited upon triple combination treatment with MEKi, AKTi, and Gem, but these were short lived and all mice eventually relapsed and succumbed to their disease (median survival = 34 days, $p < 0.001$ relative to Gem monotherapy) (figures 1E and supplementary figures 1D, 1E) which is consistent with data from others [32]. Together, the short- and long-term treatment of KPC mice mirror the transient response with limited efficacy at disease control, modeling the resistance that ultimately develops to this treatment regimen in patients.

We explored whether the limited and transient response to the triple combination therapy was due to delivery and/or metabolism of Gem. While other therapies, such as Hedgehog pathway inhibitors, have been shown to alter delivery of therapies to PDA tumors [27], we observed no differences in intratumoral concentration of Gem and its metabolites, indicating the observed effect in mice was not due to alterations in Gem delivery or metabolism (supplementary figure 1F). In addition, activation of several RTKs, including EGFR, ERBB2, ERBB3, IGF-1R, INS-R, and MET has been previously implicated in the acquisition of resistance to single agent targeting of MEK or AKT [16–20]. Based on this data, we set to investigate whether the activation of RTKs occurs upon dual MEK and AKT blockade *in vivo*. For this purpose, we evaluated the phosphorylation status of 39 RTKs (figure 1F and supplementary figure 2A). Dual blockade of MEK and AKT had inconsistent effects on Egfr phosphorylation, but induced elevations of ErbB2 phosphorylation, relative to vehicle control (supplementary figure 2A). The triple combination of Gem, MEKi, and AKTi also elicited elevation of Egfr and ErbB2 phosphorylation relative to Gem monotherapy ($n = 3/3$) while other RTK phosphorylation changes were inconsistent (figure 1F).

Taken together, our results show that the combination of MEK and AKT pathways has a modest effect on survival in mice, and that the activation of ErbB signaling occurs in mouse PDA in response to inhibition of the MEK and AKT pathways.

ERBB family signaling is activated as a malignant-specific resistant mechanism in response to MEK and AKT inhibition

To study the biochemical adaptive changes in normal or malignant contexts, we determined the efficacy of MEKi and AKTi in murine organoid cultures [22]. Organoids were generated from healthy, non-transformed epithelial cells of mouse normal pancreata (mN, n = 3), and pancreatic tumors (mT) from the KPC model (n = 3). Following treatment with AKTi and MEKi for 72 hours as single agents, mT were more resistant than mN organoids (figures 2A, 2B and table 1). While mT organoids were generally more resistant to single agent treatments, the combination of MEKi and AKTi had similar efficacy in both mT and mN cultures (figure 2C and table 1).

Short-term (2hours) AKTi or MEKi treatment inhibited phosphorylation of their respective targets in both mT and mN organoids (figures 2D, 2E). Robust inhibition of S6 phosphorylation was reached only when both AKT and MEK were inhibited (figure 2D). Re-activation of AKT and ERK was observed after 60 hours of dual MEK and AKT blockade in mT organoids (figure 2D). On the other hand, both pathways remained inactivated in mN organoids (figure 2E). These data show that target inhibition is maintained in the normal organoids, but lost in the malignant context.

Next, we sought to identify RTK gene expression changes in response to MEK and AKT blockade in organoids. For this purpose, the relative abundance of mRNA encoding selected RTKs (*Egfr*, *ErbB2*, *ErbB3*, *Igf-1r*, *Ins-r* and *Met*) was measured by qRT-PCR following single or dual agent treatment for 72 hours. Expression of *Egfr* mRNA was significantly induced in mT but not mN organoids following single and dual agent treatments for 72 hours relative to the vehicle controls (figure 2F). The gene expression levels of other RTKs were not consistently affected by any of the treatments.

To evaluate the activation status of RTKs, we measured their total and phosphorylated levels in mN and mT organoids following MEK and AKT inhibition. The combination of MEKi and AKTi resulted in elevation of both total and phosphorylated *Egfr* in mT organoids (figures 2G, 2H). mN organoids similarly elevate total levels of *Egfr*, but without increased phosphorylation (figures 2G, 2H). Phosphorylation of *ErbB2* was not elevated in mT organoids following single or dual agent treatment. Comprehensive evaluation of the phosphorylation status of other RTKs confirmed the elevation in phosphorylated *Egfr* in mT organoids following dual MEK and AKT inhibition relative to vehicle controls, but no other changes in RTK activation status (figure 2I and supplementary figure 2B). Overall, these data demonstrate that the concomitant inhibition of MEK and AKT results in activation of ErbB family members in mouse pancreatic tumor-derived organoid cultures, but not their normal counterparts.

To assess whether these biochemical adaptive mechanisms translate to human PDA, we determined the *in vitro* cytotoxicity of MEKi and AKTi in human pancreatic ductal organoids [22]. Human PDA organoid cultures (*KRAS*^{G12V} mutant human tumor (hT) organoids, n = 2 and *KRAS*^{G12D} mutant human metastatic (hM) organoid culture, n = 1), and human normal (hN) organoid cultures (*KRAS*^{wt}, n = 3) were used for this study. All of these organoids responded similarly to MEKi or AKTi treatment as single agents or in

combination (figures 3A, 3B, 3C and table 1). MEKi and AKTi monotherapies inhibited MAPK and PI3K signaling, respectively, in organoid cultures within 2 hours (figure 3D).

RTK mRNA levels were evaluated in organoids after treatment with MEKi, AKTi and a combination of both for 72 hours. The mRNA levels of *ERBB2*, *ERBB3*, *IGF-1R*, and *INS-R* were highly elevated in hT/hM organoids treated with the MEKi/AKTi combination for 72 hours, relative to vehicle control, while levels of *EGFR* were not consistently changed (figures 3E and supplementary figure 2C). Following combined treatment with MEKi and AKTi, mRNA expression of *ERBB2* and *ERBB3* in hN organoids was unchanged or modestly increased relative to vehicle (figure 3F and supplementary figure 2C). Larger changes were observed in *IGF-1R*, and *INS-R* in hN organoids following dual MEK and AKT inhibition, while *EGFR* and *MET* levels did not consistently change in response to treatment in hN and hT/hM organoids (figures 3E, 3F and supplementary figure 2C). Single agent administration of MEKi did not increase the transcript levels of most RTKs in hT/hM organoids, which is in contrast to prior reports using monolayer cultures of *KRAS*-mutant colorectal and non-small cell lung cancer [17–19].

We sought to explore whether the same resistance mechanisms persist after conversion of the organoids into monolayer cultures. Upon conversion of the hM1 organoid line into a monolayer culture (hM1-2D), we found robust elevation in the mRNA levels of *EGFR*, *ERBB2*, *ERBB3*, *IGF-1R*, *INS-R* and *MET* in all treatment regimens (supplementary figure 2D). Similar results were obtained after treatment of established human PDA cell lines with MEKi and AKTi treatment (supplementary figure 2D). These data suggest that the induction of RTK gene expression by MEKi and AKTi may be dependent on the dimensional context in which it is evaluated.

To broadly evaluate RTK activation following MEK and AKT blockade, we quantified the fold change in phospho-RTK arrays following 48 hours of treatment in hN and hT/hM cultures. We observed an increase in the phosphorylation of ERBB2, IGF-1R, and INS-R in two out of the three hT/hM cultures and ERBB3 in a single hT/hM culture (figures 3G, 3H and supplementary figure 2E). In contrast, when evaluated in a monolayer context (hM1-2D), their response to dual MEK and AKT inhibition primarily resulted in the hyper-phosphorylation of EGFR and ERBB2 (supplementary figure 2G). When hN organoids were subjected to the same treatment, we detected an increase in phosphorylated IGF-1R and INS-R, but phosphorylation of ERBB family members was either unchanged or undetectable (figures 3G, 3H and supplementary figure 2F).

We then confirmed the activation of ERBB receptors in hT/hM organoids using western blot analyses. Single and/or dual MEKi and AKTi administration for 72 hours increased total and phosphorylated ERBB2 and ERBB3 in hT/hM organoids, while EGFR phosphorylation was unchanged (figures 3I, 4H and supplementary figure 2H).

Different ERBB family members are activated in the mouse and human monolayer culture, organoid, and mouse model systems. Regardless, the pathway as a whole was consistently hyper-activated in response to dual MEK and AKT blockade. On the other hand, activation of INS-R and IGF-1R occurs regardless of neoplastic status following dual blockade of

MEK and AKT. Taken together, the tumor-specific, universal, and overall activation of ERBB signaling as a resistance mechanism to MEK and AKT inhibition across all models nominate this pathway as a therapeutic target.

ERBB blockade increases the sensitivity to MEK and AKT inhibition in mouse and human tumor organoids

The human organoid data suggest that heterodimeric complexes involving ERBB2/ERBB3 are putative mediators of resistance to MEK and AKT inhibition in PDA, whereas in mouse organoids the feedback to dual MEK and AKT blockade results in activation of Egfr. Therefore, we compared the *in vitro* efficacy of an irreversible pan-ERBB kinase inhibitor (neratinib, ERBBi) to an EGFR-specific inhibitor (erlotinib, EGFRi). Both mouse and human tumor organoids were more sensitive to ERBBi than EGFRi (supplementary figure 3A and table 1). However, while both ERBBi and EGFRi sensitized mT organoids to MEKi or AKTi (figures 4A – C and table 1), ERBBi was more efficient than EGFRi in sensitizing hT/hM cultures to either MEK or AKT inhibition (figures 4D – F and table 1).

ERBBi also significantly increased the sensitivity of both mouse and human PDA organoids to the combination of MEKi and AKTi (figures 4C, 4F). Pan-ERBB inhibition prevented hyper-phosphorylation of EGFR in mT organoids and elevated phosphorylation of ERBB2 and ERBB3 in hT/hM organoids following MEKi and AKTi treatment (figure 4G, 4H). The re-acquisition of ERK, AKT, and S6 phosphorylation induced by prolonged MEKi and AKTi treatment was averted by addition of ERBB inhibition in both mouse and human tumor organoids despite elevation of total protein levels (figures 4G, 4H).

Treatment with both MEK and AKT inhibitors has been reported to exhibit severe and common dose-limiting toxicities in the clinic [13, 33]. Therefore, we assessed the tolerability of the triple combination of MEKi, AKTi, and ERBBi in C57Bl/6J mice with two different dose levels (n = 3 for each dose level). Treatment with all three inhibitors led to severe adverse reactions and all mice succumbed within 4 to 7 days of treatment (data not shown), discouraging further exploration of this therapeutic strategy *in vivo*.

To avert the extreme toxicities associated with inhibition of MEK, AKT, and ERBB signaling, we evaluated the efficacy of alternative combinations. Synergy studies are more amenable in culture than *in vivo*. Therefore, we chose to further investigate the efficacy of the alternative combinations in organoids before proceeding to mouse studies. As an alternative to the combination of all three inhibitors, we examined the efficacy of ERBBi in combination with single agent MEKi or AKTi relative to the combination of all three antagonists. While combination of ERBBi and AKTi was not as effective as the triple combination, dual administration of ERBBi with MEKi was sufficient to achieve maximal levels of cytotoxicity (figures 5A – C and table 1). We then determined whether EGFRi and ERBBi were synergistic with either MEKi or AKTi by measuring their the combination index (CI) [26]. The CI value represents the synergistic effect of drug combinations, with CIs of <1, 1, and >1 indicating synergism, additive effects, and antagonism, respectively. The combination of ERBBi with MEKi or AKTi was synergistic in two different human PDA-derived organoids (hM1 and hT3) at high levels of fraction affected (figure 5D, 5E and table 2). Treatment with the combination of EGFRi with AKTi or MEKi was inconsistent

and antagonistic, respectively. Following long-term (60 hours) exposure to combined MEKi and ERBBi treatment, the phosphorylation of EGFR, ERK, and S6 remained inhibited, indicating successful and sustained attenuation of pathway (figure 5F). Altogether, these data suggest that synergy between MEK and pan-ERBB pathway inhibition will be efficacious *in vivo*.

Given the synergy between MEK and pan-ERBB pathway inhibition in human cells, we evaluated the efficacy of the ERBBi and MEKi combination therapy in orthotopic xenografts of human tumor organoids. Following orthotopic transplantation of hT3 organoids into NSG mice, the resulting tumors were then passaged once to generate sufficient animals for a short-term intervention study. This transplantation model recapitulates the histology of the primary tumor used to generate the organoid cultures (supplementary figure 3B). Mice were enrolled in a 7-day trial once their tumor reached a minimum volume of 350mm³ (supplementary figure 3C – D). No significant change in tumor growth was observed upon treatment with single agent ERBBi or MEKi (figures 5G, supplementary figure 3E). In contrast, inhibition of both MEK and ERBB resulted in robust regressions in all mice measured (figures 5G, supplementary figure 3E). Although we found that the ERBBi reduced cell proliferation by Ki67 immunohistochemistry (IHC), the MEKi did not have any significant impact on the number of Ki67 positive cells (figure 5G, supplementary figure 3F). In contrast, the ERBBi had no effect on cell death, but the MEKi significantly increased the number of cells positive for CC3 by IHC (figure 5G, supplementary figure 3G). Importantly, this model predicts that the therapeutic combination of MEK and pan-ERBB inhibition may be clinically useful.

CONCLUSION/DISCUSSION

In this study, we investigated the potential of a recently developed three-dimensional organoid culture system to serve as a platform for the identification of effective therapeutic strategies in PDA [22]. To identify strategies to avert acquisition of resistance without causing excessive adverse side effects, we focused on the evaluation of tumor-specific resistance pathways to combined MEK and AKT inhibition.

EGFR/ERBB and IGF-1R have been identified as resistance mechanisms to dual MEK and AKT blockade and are considered therapeutic targets for PDA [19, 34, 35]. Using mouse models and the pancreatic organoid culture system, we identified a similar response to this treatment strategy. However, it was previously unclear whether the ability to evade MEK and/or AKT inhibition was a unique property of cancer cells because of the inability to propagate normal, non-transformed pancreatic epithelial cells in the same media conditions. The organoid system enables culture of both normal non-transformed cells as well as malignant cells in the same media. With this comparator, we were able to determine that elevation of IGF-1R and INS-R phosphorylation in response to MEK and AKT inhibition is common to both normal and malignant cells. Therefore, targeting these pathways may result in deleterious and dose-limiting side effects. Although we found that both 2D culture and organoid models identified ERBB signaling as a resistance mechanism, we were able to distinguish common cellular responses observed in both normal and tumor cells versus a resistance mechanism unique to the malignant state only using the organoid model. This

advantage enabled us to prioritize targeting the ERBB signaling pathway as it was not activated in normal organoids following MEK and AKT inhibition rather than the INS-R and IGFR signaling pathways that were activated in both normal and malignant organoids.

In line with this, EGFR and ERBB2 are activated *in vivo* following therapeutic challenge with MEKi and AKTi in tumor-bearing KPC mice. Combination of a pan-ERBB kinase inhibitor with a MEK antagonist was synergistic in human tumor organoids and resulted in a robust increase in cytotoxicity. Therefore, we evaluated the therapeutic combination of MEKi and ERBBi in xenografts of human tumor organoids. Previously, we established human organoid-based orthotopic xenograft models in which tumors derived from organoids faithfully recapitulate PDA progression and pathophysiological features of human PDA tissues [22] unlike tumors derived from cell-based and/or subcutaneous xenografts. In order to accelerate our ability to evaluate the efficacy of new combination treatment strategies *in vivo*, we developed a second generation-organoid xenograft model where the organoid-derived tumor pieces were passaged and transplanted into the pancreata of immunocompromised mice. This xenograft model mimics the desmoplasia observed in human PDA and serves as a rapid-platform for therapeutic intervention studies. We found that combination of MEKi and ERBBi resulted in robust tumor regression in a second-generation organoid-based xenograft model.

Interestingly, a recent publication described the results of a Phase II trial of selumetinib (MEKi) plus erlotinib (EGFRi) in chemotherapy-refractory, advanced PDA [36]. The results of the trial showed no objective response in any of the 46 treated patients, which is consistent with our *in vitro* findings that EGFRi alone is not sufficient to sensitize human PDA organoids to MEK inhibition. These results suggest that evaluation of these biochemical adaptive changes in different culture models yields a more comprehensive prediction of the pathways utilized in acquisition of resistance to targeted agents. In addition, a new allosteric AKT inhibitor in combination with the Erk inhibitor, trametinib, has shown 1 durable partial response out of 3 patient-derived xenografts of KRAS-mutant PDA [37]. Together, our and others' data from monolayer cultures combined with the data from our organoid and *in vivo* experiments suggest that complete abrogation of ERBB signaling is required to circumvent resistance. Along these lines, treatment with an EGFR/ERBB2 inhibitor (lapatinib) that also attenuated ERBB3 phosphorylation in combination with a MEK inhibitor (trametinib) exhibited anti-tumor activity relative to monotherapies in PDA xenografts [38]. Recently, two independent groups showed that cotreatment with pan-ERBB inhibitors (neratinib and/or afatinib) and MEK inhibitors can impair *Kras*-driven lung tumorigenesis, which is also consistent with our therapeutic studies with MEKi and ERBBi in xenografts of human PDA organoids [39, 40]. These results strengthen the conclusion that combination of a pan-ERBB inhibitor with MEK antagonists may improve patient outcome.

Supplementary Material

Refer to Web version on PubMed Central for supplementary material.

ACKNOWLEDGMENTS

We thank Frances Connor, Paul Mackin, and Lisa Young for maintenance and management of mouse colonies, as well staff from the Cambridge Institute BRU, histology core, and pharmacokinetics core. MK2206 concentrations were measured by Hiroshi Hirai of Merck Research Laboratories. This research was supported by the University of Cambridge and Cancer Research UK, The Li Ka Shing Foundation and Hutchison Whampoa Limited and the NIHR Cambridge Biomedical Research Centre. KKF was supported under the NIH Ruth L. Kirschstein National Research Service Award F32CA123887-01, and KKF and DAT were supported by the European Community Grant EPC-TM-Net 256974. TB was supported by Cancer Research UK. DIJ is a Group Leader in the Cancer Research UK Cambridge Research Institute.

DAT is a distinguished scholar of the Lustgarten Foundation and Director of the Lustgarten Foundation-designated Laboratory of Pancreatic Cancer Research. This work was performed with assistance from the Animal, Microscopy, Animal and Tissue Imaging, and DNA Sequencing CSHL Cancer Center Shared Resources, which are supported by the Cancer Center Support Grant 5P30CA045508. DAT is also supported by the Cold Spring Harbor Laboratory Association, and the PMRA. This research was also supported by a Stand Up To Cancer Phillip A. Sharp Innovation in Collaboration Award, Grant Number SU2C-AACR-PS09 (to DAT). Stand Up to Cancer is a division of the Entertainment Industry Foundation, administered by the American Association for Cancer Research. In addition, we are grateful for support from the following – the Cold Spring Harbor Laboratory and Northwell Affiliation (Project Lazarus for DAT), the STARR foundation (I7-A718 for DAT), DOD (W81XWH-13-PRCRP-IA for DAT), the Associazione Italiana Ricerca sul Cancro (AIRC-18718, for VC), Sociedad Española de Oncología Médica (SEOM for MPS), the Swedish Research Council (537-2013-7277 for DÖ), The Kempe Foundations (JCK-1301 for DÖ) and the Swedish Society of Medicine (SLS-326921, SLS-250831 for DÖ), the Damon Runyon Cancer Research Foundation (DRG-2165-13 for IICC), and the NIH (5P30CA45508-26, 5P50CA101955-07, 1U10CA180944-01, 5U01CA168409-3, 1R01CA190092-01 and 1R01CA188134-01A1 for DAT; R50CA211506 for YP, F32CA180717 for CIH, 5T32CA148056 for LAB and DDE; 1K99CA204725-01A1 for DDE, P50CA101955 UAB / UMN SPORE for LAB.

REFERENCES:

1. Siegel RL, Miller KD, and Jemal A, Cancer statistics, 2018. *CA Cancer J Clin*, 2018 68(1): p. 7–30. [PubMed: 29313949]
2. Ryan DP, Hong TS, and Bardeesy N, Pancreatic adenocarcinoma. *N Engl J Med*, 2014 371(11): p. 1039–49. [PubMed: 25207767]
3. Biankin AV, et al., Pancreatic cancer genomes reveal aberrations in axon guidance pathway genes. *Nature*, 2012 491(7424): p. 399–405. [PubMed: 23103869]
4. Pylayeva-Gupta Y, Grabocka E, and Bar-Sagi D, RAS oncogenes: weaving a tumorigenic web. *Nat Rev Cancer*, 2011 11(11): p. 761–74. [PubMed: 21993244]
5. Guerra C, et al., Chronic pancreatitis is essential for induction of pancreatic ductal adenocarcinoma by K-Ras oncogenes in adult mice. *Cancer Cell*, 2007 11(3): p. 291–302. [PubMed: 17349585]
6. Hingorani SR, et al., Preinvasive and invasive ductal pancreatic cancer and its early detection in the mouse. *Cancer Cell*, 2003 4(6): p. 437–50. [PubMed: 14706336]
7. Aguirre AJ, et al., Activated Kras and Ink4a/Arf deficiency cooperate to produce metastatic pancreatic ductal adenocarcinoma. *Genes & development*, 2003 17(24): p. 3112–26. [PubMed: 14681207]
8. AMG 510 First to Inhibit “Undruggable” KRAS. *Cancer Discovery*, 2019.
9. Jones S, et al., Core signaling pathways in human pancreatic cancers revealed by global genomic analyses. *Science*, 2008 321(5897): p. 1801–6. [PubMed: 18772397]
10. Cox AD, et al., Drugging the undruggable RAS: Mission possible? *Nat Rev Drug Discov*, 2014 13(11): p. 828–51. [PubMed: 25323927]
11. Alagesan B, et al., Combined MEK and PI3K inhibition in a mouse model of pancreatic cancer. *Clin Cancer Res*, 2015 21(2): p. 396–404. [PubMed: 25348516]
12. Junttila MR, et al., Modeling targeted inhibition of MEK and PI3 kinase in human pancreatic cancer. *Mol Cancer Ther*, 2015 14(1): p. 40–7. [PubMed: 25376606]
13. Tolcher AW, et al., Antitumor activity in RAS-driven tumors by blocking AKT and MEK. *Clin Cancer Res*, 2015 21(4): p. 739–48. [PubMed: 25516890]
14. Zhong H, et al., Synergistic effects of concurrent blockade of PI3K and MEK pathways in pancreatic cancer preclinical models. *PLoS One*, 2013 8(10): p. e77243. [PubMed: 24130864]

15. Chung V, et al., Effect of Selumetinib and MK-2206 vs Oxaliplatin and Fluorouracil in Patients With Metastatic Pancreatic Cancer After Prior Therapy: SWOG S1115 Study Randomized Clinical Trial. *JAMA Oncol*, 2017 3(4): p. 516–522. [PubMed: 27978579]
16. Chandarlapaty S, et al., AKT inhibition relieves feedback suppression of receptor tyrosine kinase expression and activity. *Cancer Cell*, 2011 19(1): p. 58–71. [PubMed: 21215704]
17. Serra V, et al., PI3K inhibition results in enhanced HER signaling and acquired ERK dependency in HER2-overexpressing breast cancer. *Oncogene*, 2011 30(22): p. 2547–57. [PubMed: 21278786]
18. Turke AB, et al., MEK inhibition leads to PI3K/AKT activation by relieving a negative feedback on ERBB receptors. *Cancer Res*, 2012 72(13): p. 3228–37. [PubMed: 22552284]
19. Pettazoni P, et al., Genetic events that limit the efficacy of MEK and RTK inhibitor therapies in a mouse model of KRAS-driven pancreatic cancer. *Cancer Res*, 2015 75(6): p. 1091–101. [PubMed: 25736685]
20. Sun C, et al., Intrinsic resistance to MEK inhibition in KRAS mutant lung and colon cancer through transcriptional induction of ERBB3. *Cell Rep*, 2014 7(1): p. 86–93. [PubMed: 24685132]
21. Hayes TK, et al., Long-Term ERK Inhibition in KRAS-Mutant Pancreatic Cancer Is Associated with MYC Degradation and Senescence-like Growth Suppression. *Cancer Cell*, 2016 29(1): p. 75–89. [PubMed: 26725216]
22. Boj SF, et al., Organoid models of human and mouse ductal pancreatic cancer. *Cell*, 2015 160(1-2): p. 324–38. [PubMed: 25557080]
23. Huch M, et al., Unlimited in vitro expansion of adult bi-potent pancreas progenitors through the Lgr5/R-spondin axis. *EMBO J*, 2013 32(20): p. 2708–21. [PubMed: 24045232]
24. Hingorani SR, et al., Trp53R172H and KrasG12D cooperate to promote chromosomal instability and widely metastatic pancreatic ductal adenocarcinoma in mice. *Cancer Cell*, 2005 7(5): p. 469–83. [PubMed: 15894267]
25. Huch M, et al., Unlimited in vitro expansion of adult bi-potent pancreas progenitors through the Lgr5/R-spondin axis. *The EMBO journal*, 2013: p. 2708–2721. [PubMed: 24045232]
26. Chou TC, Theoretical basis, experimental design, and computerized simulation of synergism and antagonism in drug combination studies. *Pharmacol Rev*, 2006 58(3): p. 621–81. [PubMed: 16968952]
27. Olive KP, et al., Inhibition of Hedgehog signaling enhances delivery of chemotherapy in a mouse model of pancreatic cancer. *Science*, 2009 324(5933): p. 1457–61. [PubMed: 19460966]
28. Yeh TC, et al., Biological characterization of ARRY-142886 (AZD6244), a potent, highly selective mitogen-activated protein kinase kinase 1/2 inhibitor. *Clin Cancer Res*, 2007 13(5): p. 1576–83. [PubMed: 17332304]
29. Li D, et al., Bronchial and peripheral murine lung carcinomas induced by T790M-L858R mutant EGFR respond to HKI-272 and rapamycin combination therapy. *Cancer Cell*, 2007 12(1): p. 81–93. [PubMed: 17613438]
30. Jacobetz MA, et al., Hyaluronan impairs vascular function and drug delivery in a mouse model of pancreatic cancer. *Gut*, 2013 62(1): p. 112–20. [PubMed: 22466618]
31. Bapiro TE, et al., Gemcitabine diphosphate choline is a major metabolite linked to the Kennedy pathway in pancreatic cancer models in vivo. *Br J Cancer*, 2014 111(2): p. 318–25. [PubMed: 24874484]
32. Awasthi N, et al., Dual inhibition of the PI3K and MAPK pathways enhances nab-paclitaxel/ gemcitabine chemotherapy response in preclinical models of pancreatic cancer. *Cancer Lett*, 2019 459: p. 41–49. [PubMed: 31153980]
33. Do K, et al., Biomarker-driven phase 2 study of MK-2206 and selumetinib (AZD6244, ARRY-142886) in patients with colorectal cancer. *Invest New Drugs*, 2015 33(3): p. 720–8. [PubMed: 25637165]
34. Faller BA and Burtneis B, Treatment of pancreatic cancer with epidermal growth factor receptor-targeted therapy. *Biologics*, 2009 3: p. 419–28. [PubMed: 19774209]
35. Kindler HL, et al., A randomized, placebo-controlled phase 2 study of ganitumab (AMG 479) or conatumumab (AMG 655) in combination with gemcitabine in patients with metastatic pancreatic cancer. *Ann Oncol*, 2012 23(11): p. 2834–42. [PubMed: 22700995]

36. Ko AH, et al., A Multicenter, Open-Label Phase II Clinical Trial of Combined Mek Plus Egfr Inhibition for Chemotherapy-Refractory Advanced Pancreatic Adenocarcinoma. *Clin Cancer Res*, 2015.
37. Weisner J, et al., Preclinical Efficacy of Covalent-Allosteric AKT Inhibitor Borussertib in Combination with Trametinib in KRAS-mutant Pancreatic and Colorectal Cancer. *Cancer Res*, 2019.
38. Walters DM, et al., Inhibition of the growth of patient-derived pancreatic cancer xenografts with the MEK inhibitor trametinib is augmented by combined treatment with the epidermal growth factor receptor/HER2 inhibitor lapatinib. *Neoplasia*, 2013 15(2): p. 143–55. [PubMed: 23441129]
39. Kruspig B, et al., The ERBB network facilitates KRAS-driven lung tumorigenesis. *Sci Transl Med*, 2018 10(446).
40. Moll HP, et al., Afatinib restrains K-RAS-driven lung tumorigenesis. *Sci Transl Med*, 2018 10(446).

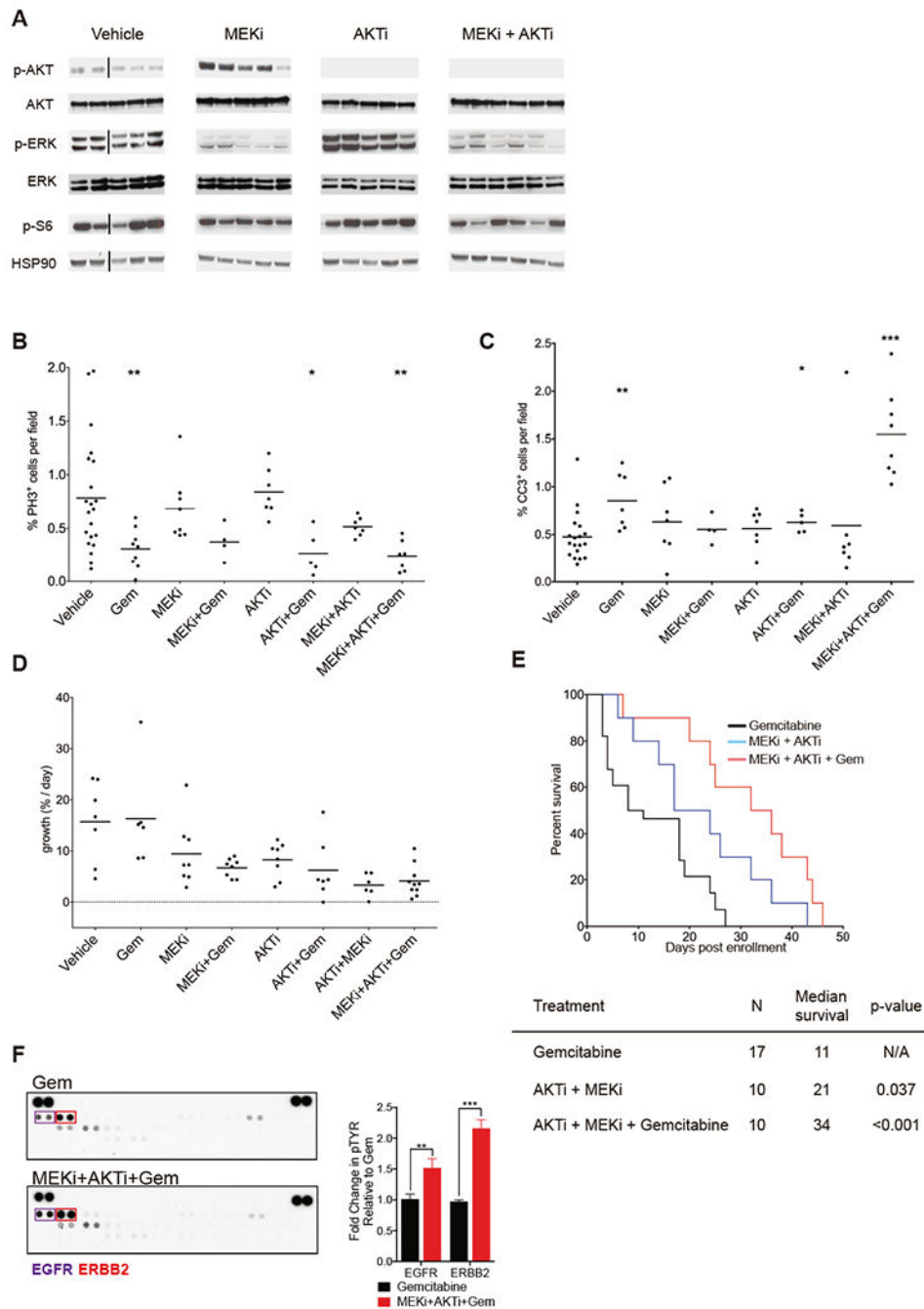


Figure 1. Analysis of the efficacy of combined treatment with MEK and AKT inhibitors in a mouse model of pancreatic cancer.

A) *Kras^{+LSL-G12D}; Trp53^{+LSL-R172H}; Pdx1-Cre* (KPC) mice were treated for 7 days with vehicle, MEKi, AKTi or a combination of MEKi and AKTi. Five tumors per group were analyzed by immunoblot for activation of the respective signaling pathways. Hsp90 is used as a loading control. The line separates different blots. **B)** Percentage of proliferating cells within the tumor mass was measured by staining tissue sections from KPC treated mice for phospho-histone H3 (PH3). Lines indicate mean percentage values. * p<0.05, ** p<0.01, *** p<0.001.

and *** $p < 0.001$ relative to vehicle control by one-way ANOVA with Dunnett's multiple comparison test and single pooled variance. **C)** Percentage of apoptotic cells for cleaved caspase (CC3), presented as in **B**. **D)** Percentage of tumor growth (shown as percentage per day) for the different treatment groups. Lines indicate mean growth values. * $p < 0.05$, ** $p < 0.01$, and *** $p < 0.001$ relative to vehicle control by one-way ANOVA with Dunnett's multiple comparison test and single pooled variance. **E)** Survival curves of KPC mice treated with vehicle, Gemcitabine, MEKi + AKTi or with MEKi + AKTi + Gemcitabine. **F)** Quantification of changes in phosphorylation of Egfr and ErbB2 detected by phospho-RTK array is displayed on the right, with error bars indicating standard deviation of the means.

Author Manuscript

Author Manuscript

Author Manuscript

Author Manuscript

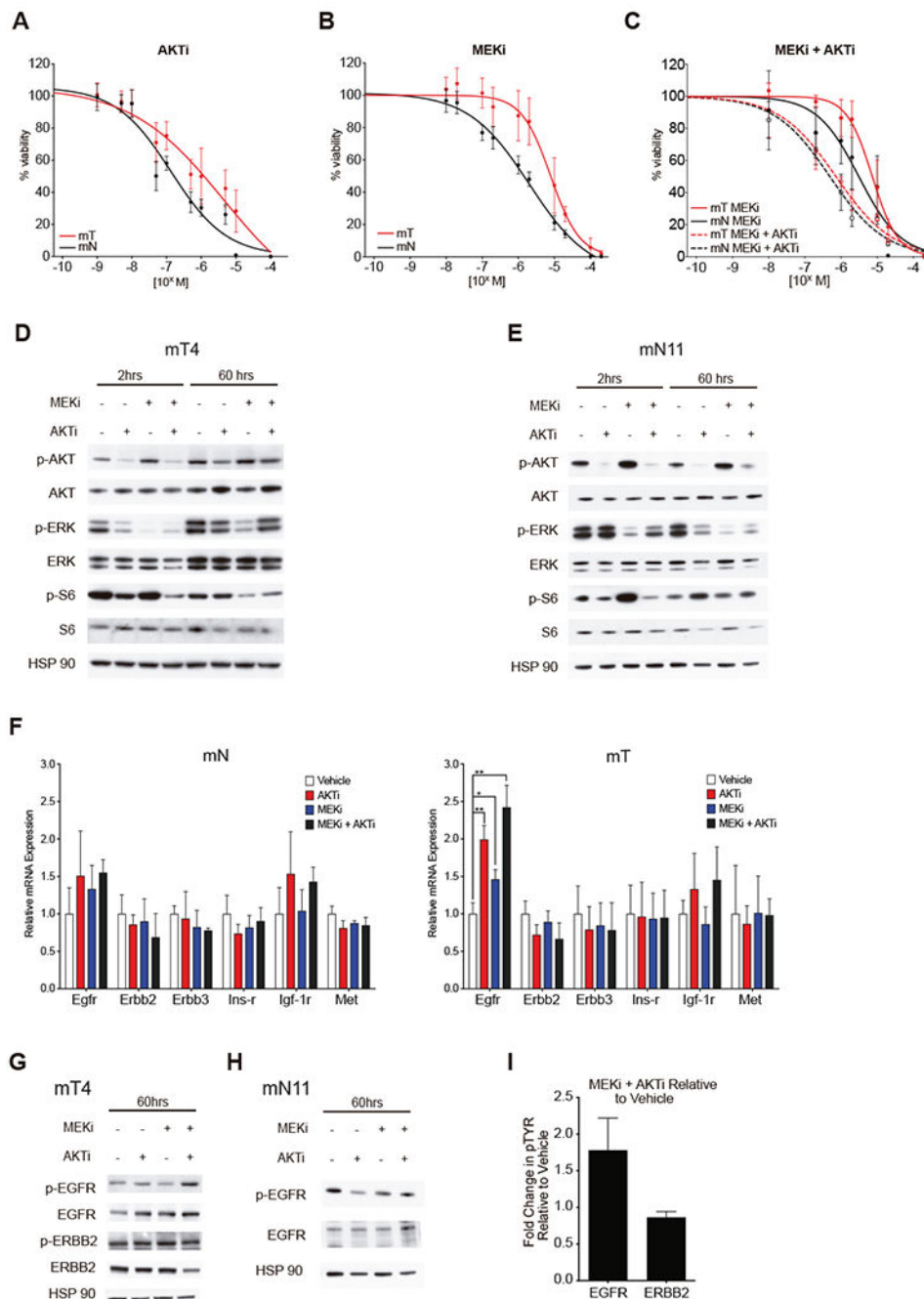


Figure 2. MEK and AKT inhibition promotes Egfr expression and phosphorylation in murine pancreatic organoids.

A-C) Dose-response curves of mN and mT organoids treated with AKTi alone (A), MEKi alone (B), and MEKi or a combination of both AKTi and MEKi (C). n = 3 for each group. Error bars indicated standard deviation. **D-E)** Immunoblot analysis of MEK and AKT pathway status in mT organoids (D) and mN organoids (E) treated for 2 or 60 hours with single or combination therapies. Hsp90 is shown as a loading control. **F)** Changes in mRNA levels of ErbB receptors and other RTKs measured by qRT-PCR in mN and mT organoids,

following treatment for 72 hours with single and dual inhibition of MEK and AKT. n = 3 per group (* p<0.05, ** p<0.01, and ***p<0.001). **G-H**) Immunoblot analysis of ErbB pathway activation status in mT organoids (G), and Egfr activation status in mN organoids (H) treated for 60 hours with single or combination therapies. Hsp90 is shown as a loading control. Hsp90 is shown as a loading control. **I**) Quantification of Phospho-RTK array for mT organoids treated for 48 hours with either DMSO (vehicle) or MEKi and AKTi. Changes in phospho-RTK levels are quantified, error bars indicate standard deviation of the means.

Author Manuscript

Author Manuscript

Author Manuscript

Author Manuscript

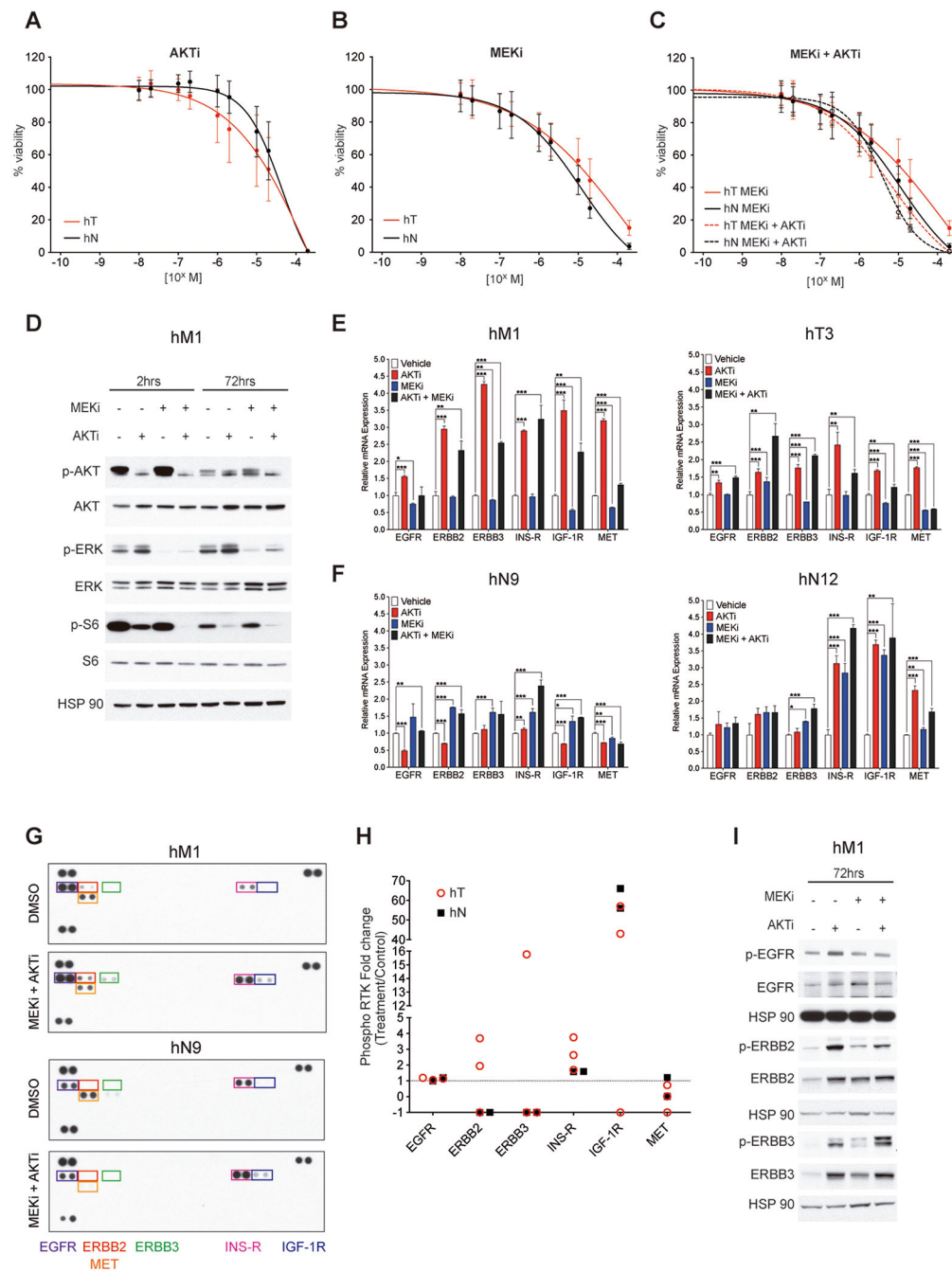


Figure 3. Combined inhibition of MEK and AKT promotes ERBB2/3 expression and phosphorylation in human pancreatic organoids.

A-C) Dose-response curves of human T organoids (hT) and human normal organoids (hN) treated with AKTi (A) and MEKi (B), and MEKi + AKTi (C). n=3 per each group. **D)** Immunoblot analysis of MEK and AKT pathway activation status in hM1 organoids treated for 2 or 72 hours with single or combination therapies. Hsp90 is shown as a loading control. **E-F)** Changes in mRNA levels of ERBB family members and other RTKs in hT organoids (E) and hN organoids (F) following 72-hour treatment with MEK and AKT inhibitors as

single agents or in combination. n = 3 per group (* p<0.05, ** p<0.01, and ***p<0.001). **G)** Representative phospho-RTK arrays for human tumor and normal organoids. **H)** Quantification of changes in phospho-RTK levels after treatment with the combination of MEKi and AKTi for 48 hours relative to DMSO controls. Values less than 0 indicate non-detectable signal. **I)** Immunoblot analysis of ERBB pathway activation status hM1 organoids treated for 72 hours with single or combination therapies. Hsp90 is shown as a loading control.

Author Manuscript

Author Manuscript

Author Manuscript

Author Manuscript

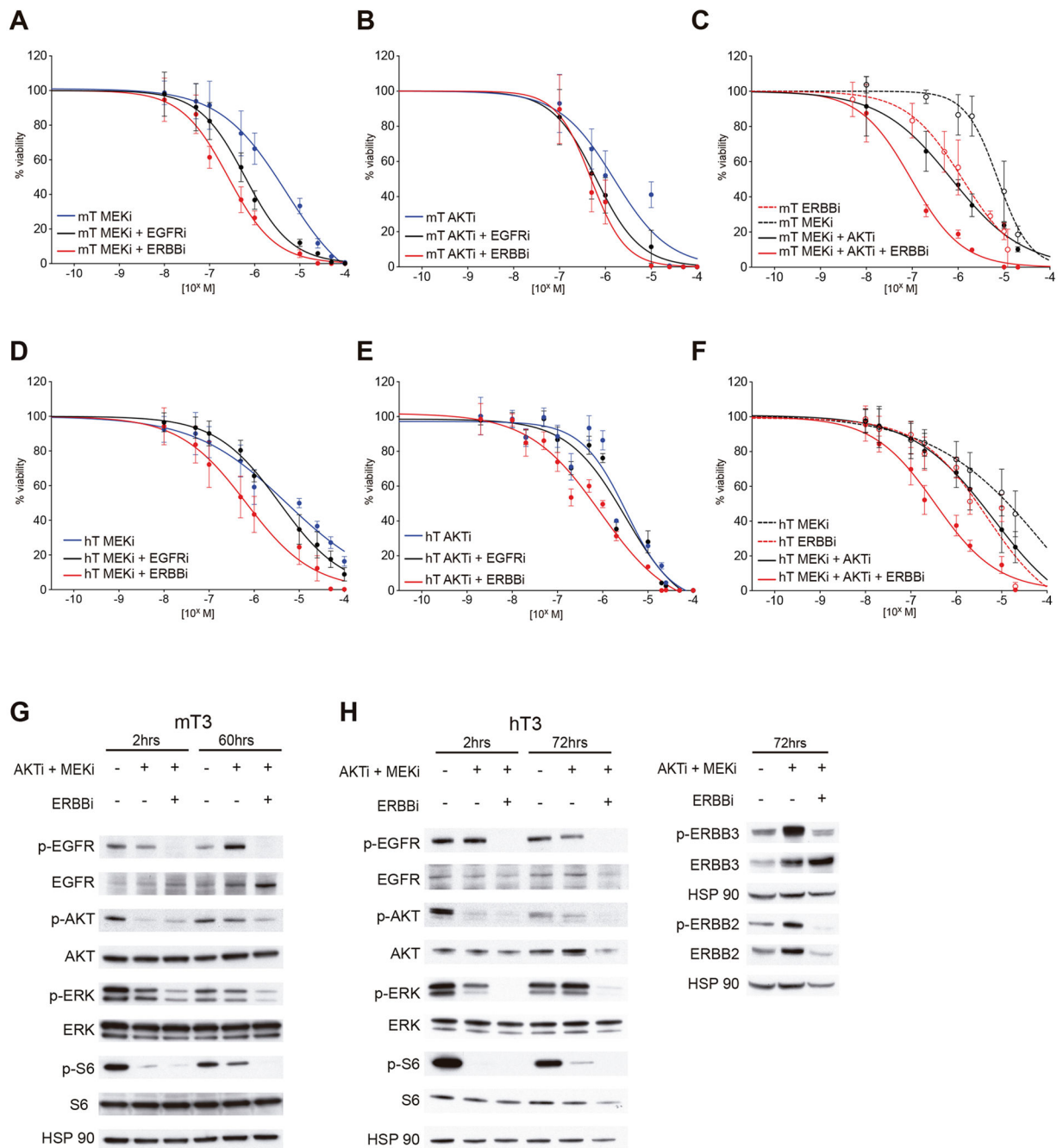


Figure 4. Pan-ERBB kinase inhibition is more effective than EGFR inhibition alone in human tumor organoids.

A-C) Dose-response curves of mT organoids (n = 3) treated with MEKi, MEKi + EGFRi, or MEKi + ERBBI (A), AKTi, AKTi + EGFRi, or AKTi + ERBBI (B), MEKi, ERBBI, MEKi + AKTi, or MEKi + AKTi + ERBBI (C). For all dose response curves, error bars represent standard deviation. **D-F)** Dose-response curves of hT organoids (n = 3) treated with MEKi, MEKi + EGFRi, or MEKi + ERBBI (D), AKTi, AKTi + EGFRi, or AKTi + ERBBI (E), and MEKi, ERBBI, MEKi + AKTi, or MEKi + AKTi + ERBBI (F). For all dose response curves,

error bars represent standard deviation. **G)** Immunoblot analysis of mT3 organoids treated for 2 or 60 hours with MEKi + AKTi or MEKi + AKTi + ERBBI. Hsp90 is shown as a loading control. **H)** Immunoblot analysis of hT3 organoids treated for 2 or 72 hours with MEKi + AKTi or MEKi + AKTi + ERBBI.

Author Manuscript

Author Manuscript

Author Manuscript

Author Manuscript

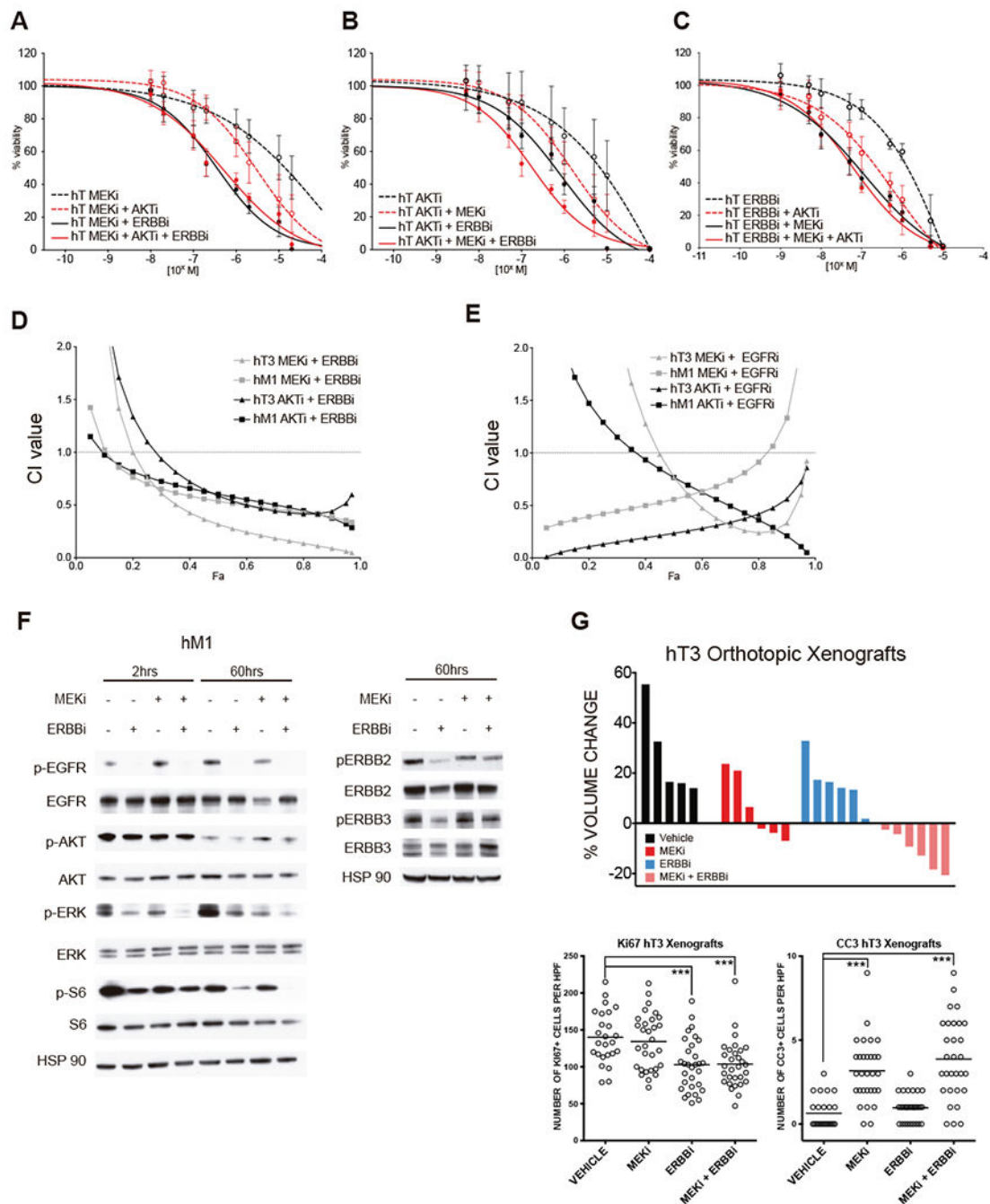


Figure 5. Combination of Pan-ERBB kinase and MEK inhibitors achieves similar efficacy to the triple combination.

A-C) Dose-response curves of hT (n = 3) organoids treated with MEKi, MEKi + AKTi, MEKi + ERBBi, or MEKi + AKTi + ERBBi (A), AKTi, AKTi + MEKi, AKTi + ERBBi, AKTi + MEKi + ERBBi (B), ERBBi, ERBBi + AKTi, ERBBi + MEKi, or MEKi + AKTi + ERBBi (C). For all dose response curves, error bars represent standard deviation. **D-E)** CI plots for the dual combinations of MEKi + ERBBi and AKTi + ERBBi (D) and AKTi + EGFRi and MEKi + EGFRi (E) in two human PDA organoids. CI values were plotted as a

function of fractional inhibition for the fraction affected (Fa) range of 0.10 to 0.97. **F)** Immunoblot analysis of hM1 organoids treated for 2 or 60 hours with ERBBi, MEKi, or ERBBi + MEKi. Hsp90 is shown as a loading control. **G)** Waterfall plot of individual tumor volume changes as measured by ultrasound using human tumor xenografts *in vivo* treated with Pan-ERBB kinase and MEK inhibitors (upper panel). Number of proliferating cells within the tumor mass was measured by staining tissue sections from treated mice for Ki67 (lower left plot). Lines indicate mean. Number of apoptotic cells within the tumor mass was measured by staining tissue sections from treated mice for cleaved caspase (CC3) (lower right panel). * $p < 0.05$, ** $p < 0.01$, *** $p < 0.001$ and **** $p < 0.0001$ relative to vehicle control by two-tailed Mann Whitney non-parametric t test.

Table 1.

EC50 of mouse and human organoids treated with the indicated antagonists. Individual experiments are separated by a thick line. EC50 is shown as the average and the 95% CI in parenthesis.
(hT: human tumor organoids, hN: human organoids from normal pancreata, mT: mouse tumor organoids, mN: mouse organoids from normal pancreata)

Drug(s)	hT	hN	mT	mN
MEKi	11 μ M (7-15)	12 μ M (9-14)	8 μ M (6.8-9.1)	2 μ M (1.6-5.3)
AKTi	12 μ M (10-14)	70 μ M (50-90)	4.3 μ M (0.8-8)	0.14 μ M (0.1-0.2)
MEKi + AKTi	3 μ M (2.1-4.5)	3.9 μ M (2.3-5.5)	0.7 μ M (0.5-1)	0.5 μ M (0.3-0.8)
MEKi + AKTi + ERBBI	0.4 μ M (0.3-0.5)		0.1 μ M (0.07-0.15)	
MEKi + ERBBI	0.5 μ M (0.4-0.7)			
ERBBI	1.5 μ M (0.9-2.3)		1.2 μ M (0.7-1.7)	
ERBBI	1.3 μ M (1-2)		1.2 μ M (0.8-1.6)	
EGFRi	12 μ M (10-14)		5 μ M (3-7)	
AKTi	5.3 μ M (2.1-8.4)		3 μ M (2-4)	
AKTi + EGFRi	3.2 μ M (2-5.3)		0.6 μ M (0.5-0.7)	
AKTi + ERBBI	0.8 μ M (0.6-1.3)		0.5 μ M (0.4-0.6)	
MEKi	6.5 μ M (4.5-7.3)		6 μ M (5.5-7.7)	
MEKi + EGFRi	3.6 μ M (3.2-4.2)		0.6 μ M (0.5-0.7)	
MEKi + ERBBI	0.6 μ M (0.5-0.8)		0.3 μ M (0.2-0.3)	

Table 2.

Combination indexes (CI) of drug combinations in human tumor and metastatic (hT and hM) organoids.

Combination Index (CI) at:	Fa50	Fa90	Fa95	Fa97
AKTi + EGFRi				
hM1	0.96	0.40	0.30	0.25
hT3	0.43	0.75	0.92	1.06
MEKi + EGFRi				
hM1	0.75	1.53	2.21	2.98
hT3	0.97	0.53	0.80	1.15
AKTi + ERBBi				
hM1	0.60	0.37	0.32	0.28
hT3	0.59	0.43	0.52	0.59
MEKi + ERBBi				
hM1	0.54	0.38	0.35	0.33
hT3	0.31	0.09	0.06	0.04